

PlanScope: Learning to Plan Within Decision Scope Does Matter

Ren Xin, Jie Cheng, and Jun Ma

Abstract—In the context of autonomous driving, learning-based methods have been promising for the development of planning modules. During the training process of planning modules, directly minimizing the discrepancy between expert-driving logs and planning output is widely deployed. In general, driving logs consist of suddenly appearing obstacles or swiftly changing traffic signals, which typically necessitate swift and nuanced adjustments in driving maneuvers. Concurrently, future trajectories of the vehicles exhibit their long-term decisions, such as adhering to a reference lane or circumventing stationary obstacles. Due to the unpredictable influence of future events in driving logs, reasoning bias could be naturally introduced to learning based planning modules, which leads to a possible degradation of driving performance. To address this issue, we identify the decisions and their corresponding time horizons, and characterize a so-called decision scope by retaining decisions within derivable horizons only, to mitigate the effect of irrational behaviors caused by unpredictable events. This framework employs wavelet transformation based log preprocessing with an effective loss computation approach, rendering the planning model only sensitive to valuable decisions at the current state. Since frequency domain characteristics are extracted in conjunction with time domain features by wavelets, decision information across various frequency bands within the corresponding time horizon can be suitably captured. Furthermore, to achieve valuable decision learning, this framework leverages a transformer based decoder that incrementally generates the detailed profiles of future decisions over multiple steps. Our experiments demonstrate that our proposed method outperforms baselines in terms of driving scores with closed-loop evaluations on the nuPlan dataset. The source code and associated videos are available at <https://github.com/Rex-sys-hk/PlanScope>.

I. INTRODUCTION

Learning-based autonomous driving systems have been a promising approach for the popularity of unmanned vehicles. In particular, learning from driving logs of experts is broadly adopted to supervise neural networks for the planning task. During the training process, distance error is commonly employed, which is to measure the discrepancy between the planned state sequence and the expert demonstrations, thereby optimizing parameters of the neural network [1]. Yet, when training end-to-end autonomous driving systems, it is not entirely reasonable to set the logged expert states as target sequence, because future events are inherently uncertain, and potential disruptions such as unexpected obstacles or fluctuating traffic signals can significantly alter the trajectory planning. These unpredictable elements necessitate agile and nuanced adjustments to driving behavior. Some seemingly predictable decisions, such as the interaction behavior and

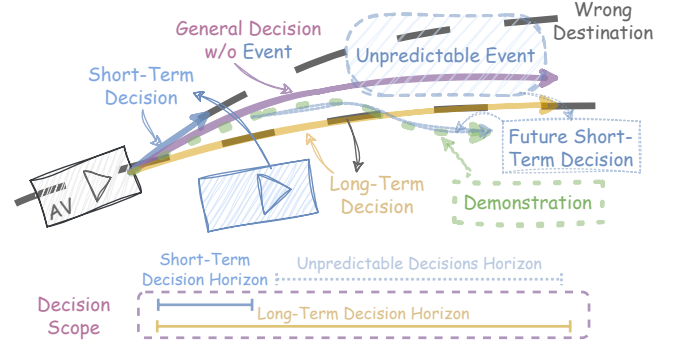


Fig. 1. In the scenario presented, the ego vehicle’s long-term decision-making is characterized by adherence to the reference line for driving. Conversely, short-term decision-making involves evading opposing vehicles through the application of lateral velocity. Long-term and short-term decisions integrate the general decision at the moment. However, the demonstrated trajectory, which anticipates future short-term decisions to avoid unpredictable events, may appear counterintuitive in the current context. The decision scope mechanism deliberately focuses on a limited horizon of short-term decisions while maintaining a broader horizon for long-term decisions, thereby mitigating the effect of unpredictable decisions in the demonstrated trajectory.

future trajectory of other traffic participants, are difficult to accurately predict. For example, when modeling the interactions by non-cooperative game theory, the decision planner converges only when observing other traffic participants respond. Otherwise, one can only avoid interactions with others to evade falling into disadvantageous states. Meanwhile, a short-sighted planner is also not desirable, as the planner also needs to keep its long-term decision in consideration when choosing sudden maneuvers. Essentially, the state sequence of experts recorded in the log is a combination of short-term and long-term decisions under different scopes. A diagram of this concept is shown in Fig. 1.

Obviously, an agent needs a broad enough view of the overall situation, handles the current trivialities, and does not overly concern about the trivialities of the future. As a reference, in traditional planning methods, the process is artificially segmented into distinct tiers according to the problem scope: path planning, behavior planning, and motion planning, with each addressed by specialized modules [2]. Conversely, learning-from-demonstration approaches typically involve directly learning future trajectories of a pre-determined length, because the nuanced adjustment components and long-term decision components cannot be directly distinguished from log replay. Driving-behavior-reasoning by manual annotation could be an approach to analyze the long-term and short-term decisions [3], by which the behavior duration and their starting time can be obtained. However, this paradigm requires a heavy workload and is typically challenging to scale up. To address the aforementioned challenges, we employ wavelet transformation to extract

Ren Xin, Jie Cheng, and Jun Ma are with The Hong Kong University of Science and Technology, Hong Kong SAR, China. (email: rxin@connect.ust.hk; jchengai@connect.ust.hk; jun.ma@ust.hk)

information at various frequency bands, enabling our model to discern the appropriate actions from log replays in a self-supervised manner. Unlike the Fourier transform, wavelet transformation utilizes basis functions of finite length, which facilitates the capture of choppy features in signals [4]. This technique employs a convolution-like process to extract signal components. Based on wavelet transformation, we propose a mechanism to learn within the decision scope, such that the time horizon of distinct frequency bands can be modulated. In this sense, we can compare the decision details generated from the neural network with decomposed details at different horizons, and this prevents the model from overextending its planning into the future. In order to render the details obtained by decomposition efficiently in model training, we introduce a decoding module that generates detailed short-term decisions at multiple detail levels recursively. Our contributions are threefold:

- We introduce a novel self-supervised mechanism that learns to plan within decision scope. This approach leverages wavelet decomposition, which extracts frequency domain characteristics in conjunction with time domain features, to capture motion information across various scales within the corresponding time horizon.
- We propose a new transformer based Iterative Detail Decoder (IDD) to iteratively generate the trajectory decisions and its finer details, thereby enabling models to selectively learn the trajectory intricacies.
- Our method has been rigorously evaluated on the nu-Plan [5] dataset, and the results demonstrate that it achieves superior driving scores compared to baseline methods in closed-loop evaluations, especially under critical safety related metrics.

II. RELATED WORKS

A. Horizon Related Planner Design

Sequential decision-making can be encapsulated with the framework of Partially Observable Markov Decision Processes (POMDPs) [6]. Within this paradigm, the ego agent must make decisions based on environmental observations, anticipate subsequent states following its actions, and maximize the cumulative reward. Given the world model (also known as the transition function) and the constraint of limited observations, the optimal policy can be derived by exploring the state space and resolving the Bellman equation. However, in autonomous driving scenarios, the world model is generally unknown, making it challenging to determine the optimal policy sequence incrementally in real-time [7]. Hence, under traditional planning frameworks, hierarchical structure is typically employed to streamline computations [8], [9]. In the hierarchical structure, the planning problem is decomposed across various frequency bands, each with distinct hierarchical tendencies. For large-scale exploration, one might opt for a lower resolution and focus on non-real-time targets. Conversely, within the smaller scale areas identified by the large-scale search, our planner can leverage higher resolution and account for dynamic objects that are impractical

to predict accurately. In [10], it adapts this concept to the prediction phase, and segments the forecast for the subsequent four seconds into two stages. Initially, it meticulously predicts the agent’s reachable area at 0.1-second intervals for the first 0.5 seconds. Subsequently, for the remaining 3.5 seconds, it utilizes an adaptive filter to depict potential vehicle positions. This approach allows the agent to maintain safety at a fine scale while preserving adaptability at a broader scale. In terms of learning-based planning, analogous strategies can be harnessed to simplify calculations and enhance performance. For instance, the Negative Log Likelihood (NLL) Loss, which is frequently utilized in predictive tasks [11], assigns greater uncertainty to long-term trajectory points, such that the scarcity of future information can be reflected. This phenomenon of probabilistic regression result helps to posit that historical trajectories provide limited insight, sufficient only for fine-tuned operations in the short term and for general directional guidance in the long term. However, NLL loss or probabilistic predictions are incompatible with the planning module, which necessitates deterministic outputs for trajectory followers. It leaves an open and interesting problem to develop an approach to address this trajectory planning challenge.

B. Applications of Wavelet Transformation

Wavelet transformation is a potent tool in signal processing [4], [12]. This approach has been extensively applied in medical imaging and image recognition, which demonstrates superior performance comparing to convolutional neural networks (CNNs), particularly with fewer samples [13]. Its utility can be further extended to the domain of autonomous driving, where it has been effectively harnessed. For instance, in [14], wavelet transformation is employed to distill large-scale car-following behaviors. It preprocesses the signal approximations derived by wavelet transformation, calculates affinities using Summed Square Error (SSE), and identifies three predominant behavioral patterns through hierarchical clustering. In [15], vehicle state records are analyzed by wavelet transformation to identify drivers. Wavelet coefficients, energy, and statistical quantities are concatenated to the feature vector and recognized by classifiers like XGBoost, achieving around 100% accuracy when identifying 80% drivers. In [16], rasterized high-resolution maps are decomposed into multi-resolution geometry graphs by wavelet based cell decomposition. The graph is utilized by both path and motion planning modules to improve computing efficiency. Motivated by these precedents, we advocate the application of wavelet transformation to glean valuable information from expert trajectories.

III. METHODOLOGY

Our research concentrates on addressing the problem of urban autonomous driving. At each time step, the autonomous vehicle is tasked with planning a future trajectory \mathcal{T} under various traffic-related contexts C_t . Each trajectory point has six channels: $[p_x, p_y, \cos \theta, \sin \theta, v_x, v_y]$. Driving contexts encompass dynamic agents (A), static objects (O), and Vectorized High-Definition Map (M) information. Generated outputs at time step t , denoted as G_t , include motion predictions

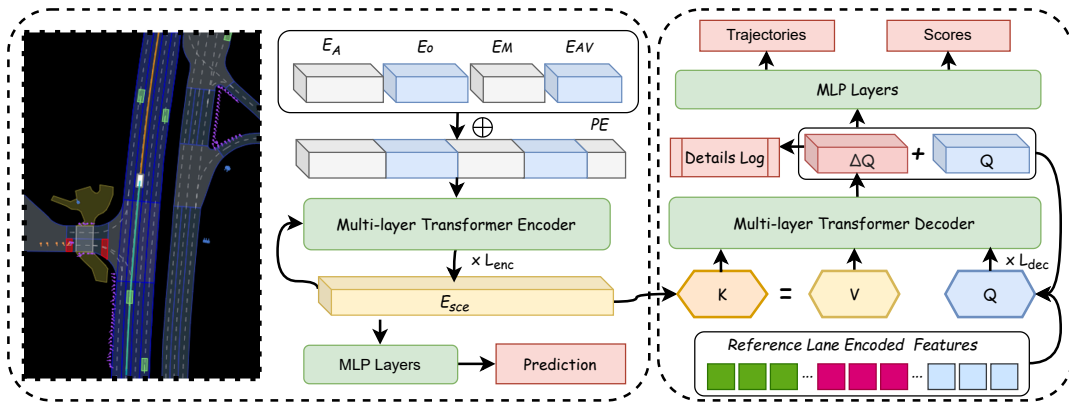


Fig. 2. The overall model framework initiates with the individual encoding of driving context elements, including the Ego Vehicle, Dynamic Agents, Static Objects, High-Definition Map, Traffic Signs, and Signals, followed by their concatenation with positional encoding (PE) [17]. This concatenated context is subsequently processed through a Multi-layer Transformer encoder, iterated L_{enc} times. The scenario encoding is then decoded to formulate agent predictions, which serve to comprehensively supervise the model’s understanding of the driving context. The reference lane encoding and anchor-free variables are combined to form a query for the scenario encoding. The decoder’s output generates residual latent variables, with each layer’s latent variable being logged as that layer’s detail and aggregated with the reference query to form the new query for the subsequent layer.

\mathcal{P} of other agents, a multimodal trajectory score \mathcal{S} , and detailed trajectory information \mathcal{D} at different levels of detail. A basic mathematical formulation of this framework can be represented as follows:

$$C_t = \{A_t, A_t - 1, \dots, O_t, M_t, AV_t\}, G_t = \{\mathcal{T}, \mathcal{P}, \mathcal{S}, \mathcal{D}\},$$

$$G_t = f(C_t|\theta), \text{ w.r.t. } \theta = \arg \min_{\theta} \mathcal{L}(G_t, \hat{G}_t),$$

where f denotes the neural network model, θ is the model parameter, \mathcal{L} is the loss function, and \hat{G}_t is the ground truth of G_t from logged context.

Driving contexts are encoded as E_A, E_o, E_M, E_{AV} by Feature Pyramid Network (FPN) [18], Multi Layer Perceptron (MLP), PointNet [19] based vector encoder and attention based State Dropout Encoder (SDE) [20] respectively. As depicted in Fig. 2, the encoder section of our framework is conventional and similar to that of the baseline prediction and planning model described in [21]. The decoder section has been meticulously designed by us. It generates trajectories that are subsequently employed as references by a Linear Quadratic Regulator (LQR). To minimize the influence of human-defined rules, we have eliminated the rule-model hybrid post-processing module in our experiments. During the training phase, various commonly utilized auxiliary losses are integrated to supervise the trajectory generation. The training losses include prediction loss \mathcal{L}_{pre} , and collision loss \mathcal{L}_{col} , which can be expressed by

$$\mathcal{L}_{pre} = \text{L1}_{smooth}(\mathcal{P}, \hat{\mathcal{P}}),$$

$$\mathcal{L}_{col} = \frac{1}{T_f} \sum_{t=1}^{T_f} \sum_{i=1}^{N_c} \max(0, R_c + \epsilon - d_i^t),$$

where \mathcal{L}_{pre} calculates the future trajectory discrepancy between generated and that from dataset, \mathcal{L}_{col} computes the invasion distance using N_c circle represented vehicle outline in future T_f steps as described in [21], R_c is the summed radius of ego and agents outline circle, ϵ is the tolerance, and d_i^t represents the center distance between outline circles at time step t . Drawing inspiration from [22]–[24], the decoder’s query

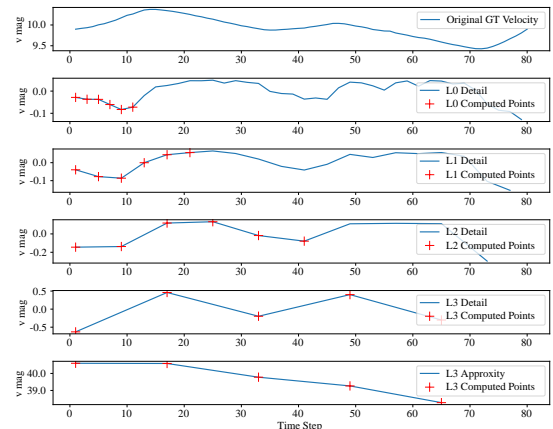


Fig. 3. Velocity along the trajectory is decomposed into different levels of detail. Only the red cross-marked data points in each level are in scope.

is formulated as a concatenation of the reference lane encoding and anchor-free variables. The reference lane encoded features are concatenated with anchor-free learnable queries and serve as the initial query Q_0 to the scenario encoding within multi-layer self-attention operations, facilitating the generation of residual quantities of Q for subsequent layers. More details on the acquisition of supervision signals and the decoding of detailed information are elaborated in Section III-A and Section III-B, respectively.

A. Expert Log Decomposition

In order to obtain decision components in the trajectory logs and selectively study them, we can decompose them through mathematical analysis tools. Fourier transform is a commonly used analysis method. It extracts the coefficient of the signal at different frequencies by convolution signal with sine and cosine functions as basis functions. However, since sine and cosine functions are infinite supporting, this decomposition will completely lose the time domain characteristics of the signal, resulting in our failing to select part of a certain time segment in each domain component. The wavelet transformation can help with this. Wavelets, also known as scale-varying basis functions, refer to a method of decomposing

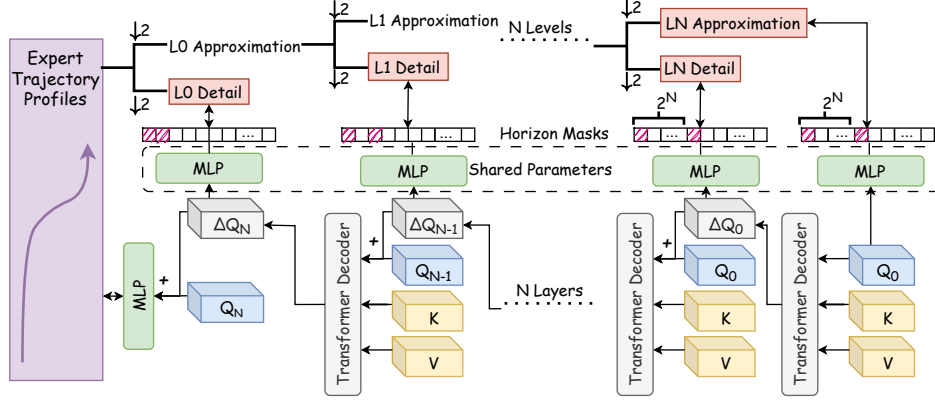


Fig. 4. The iterative detail decoder’s architecture leverages reference lane encoding as the initial query for multi-layer attention mechanisms. Detail coefficients extracted during each iteration are integrated with the preceding query to formulate the subsequent query, thereby refining the extraction of further detailed information. The initial query serves as an approximation, with the first query and the ensuing generated details being processed by an MLP. These details are then mapped and compared against the detailed components at each level of the ground truth trajectory. The profile residual values are supervised by the profile details within the decision scope. Notably, the horizon masks can be configured individually across levels.

signals using compact supporting functions as basis functions. For example, the Haar wavelet, the simplest basis function of the wavelet transformation, enjoys widespread application in signal processing. The basis functions of Haar wavelet are

$$\phi(t) = \begin{cases} 1, & 0 \leq t < 1 \\ 0, & \text{otherwise} \end{cases}, \psi(t) = \begin{cases} 1, & 0 \leq t < \frac{1}{2} \\ -1, & \frac{1}{2} \leq t < 1 \\ 0, & \text{otherwise} \end{cases}$$

where t is the discrete time index. We can see that when $t \notin [0, 1]$, the basis function value is 0, which means that the function is compact supporting. Among the basis functions, the scaling function $\phi(t)$, often referred to as the father wavelet, serves as a low-pass filter within the wavelet transform process; the mother wavelet function $\psi(t)$ is primarily utilized for extracting the high-frequency components of a signal. Through the convolution of the original signal with these basis functions, the signal’s high-frequency and low-frequency components are isolated. In the trajectory decomposition context, the trajectory approximation coefficient \mathcal{T}_A and the detail coefficient \mathcal{T}_D can be derived by performing the following transformation over the time horizon

$$\mathcal{T}_{A_t} = \sum_k \mathcal{T}[k] \phi(2t - k), \mathcal{T}_{D_t} = \sum_k \mathcal{T}[k] \psi(2t - k),$$

where $\mathcal{T}[k]$ is the discrete trajectory profile, \mathcal{T}_{A_t} is the low-frequency approximation coefficient at time index t , \mathcal{T}_{D_t} is the high-frequency detail coefficient at time index t , k can be considered as the convolution handler. This decomposition process is called Discrete Wavelet Transformation (DWT), which can be recursively applied to the approximation coefficient \mathcal{T}_A to achieve multi-level l decomposition. By

$$\left(\mathcal{T}_A^l, \mathcal{T}_D^l \right) = \text{DWT} \left(\mathcal{T}_A^{l-1} \right),$$

we decompose trajectory profiles into N levels. The approximation obtained in the last level is nominated as the preliminary decision. With extraction of a detail component in each level, the length of the data is reduced by half. An illustration of velocity decision scope diagram from log decomposition is provided in Fig. 3.

B. Iterative Detail Decoder

Since the decomposed trajectory profile has been obtained, the question arises as to how it can be effectively utilized to guide the supervision of model training process. One potential method is to reconstruct the whole trajectory by truncated detail profiles. Nevertheless, this method requires assumption of data out of horizon to be zero, which introduces more deterministic prior in supervision signal. To facilitate the learning of detailed information, IDD is designed, which is capable of progressively generating details across multiple iterations. The architecture of the IDD is depicted in Fig. 4. In the decoding process, the encoding of reference lane serves as the query Q_0 , and scenarios encoding E_{sce} serves as key and value for a series of self-attention operations. The details extracted at each iteration are accumulated with the previous query, which is then utilized as the subsequent query. This iterative accumulation allows for the acquisition of increasingly refined trajectory profile. Mathematically, the process can be described as

$$\begin{aligned} \tilde{Q}_{i-1} &= \text{SelfAttn}(Q_{i-1}, \text{dim} = 0), \\ \tilde{Q}'_{i-1} &= \text{SelfAttn}(Q'_{i-1}, \text{dim} = 1), \\ \Delta Q_i &= \text{CrossAttn}(\tilde{Q}_{i-1}, E_{sce}, E_{sce}), \\ Q_i &= \Delta Q_{i-1} + Q_{i-1}. \end{aligned}$$

In the decoding process, residual variables ΔQ_i generated during each iteration are recorded. Both Q_0 and logged ΔQ_i list are remapped by the same MLP decoder, i.e.,

$$\tilde{\mathcal{T}}_A^N = \text{MLP}(Q_0), \tilde{\mathcal{T}}_D^l = \text{MLP}(\Delta Q_{N-l}).$$

The length of $\tilde{\mathcal{T}}$ is the same as planning steps. To make sure the decoded details in same length as driving details, down sampling is performed on $\tilde{\mathcal{T}}$ by

$$\mathcal{T}_A^N = \tilde{\mathcal{T}}_A^N \downarrow 2^N, \mathcal{T}_D^l = \tilde{\mathcal{T}}_D^l \downarrow 2^{l+1}.$$

These details are compared with the corresponding components of expert trajectories at multiple levels. To get decision details in a proper scope, only limited time horizon H_l of \mathcal{T}_D^l

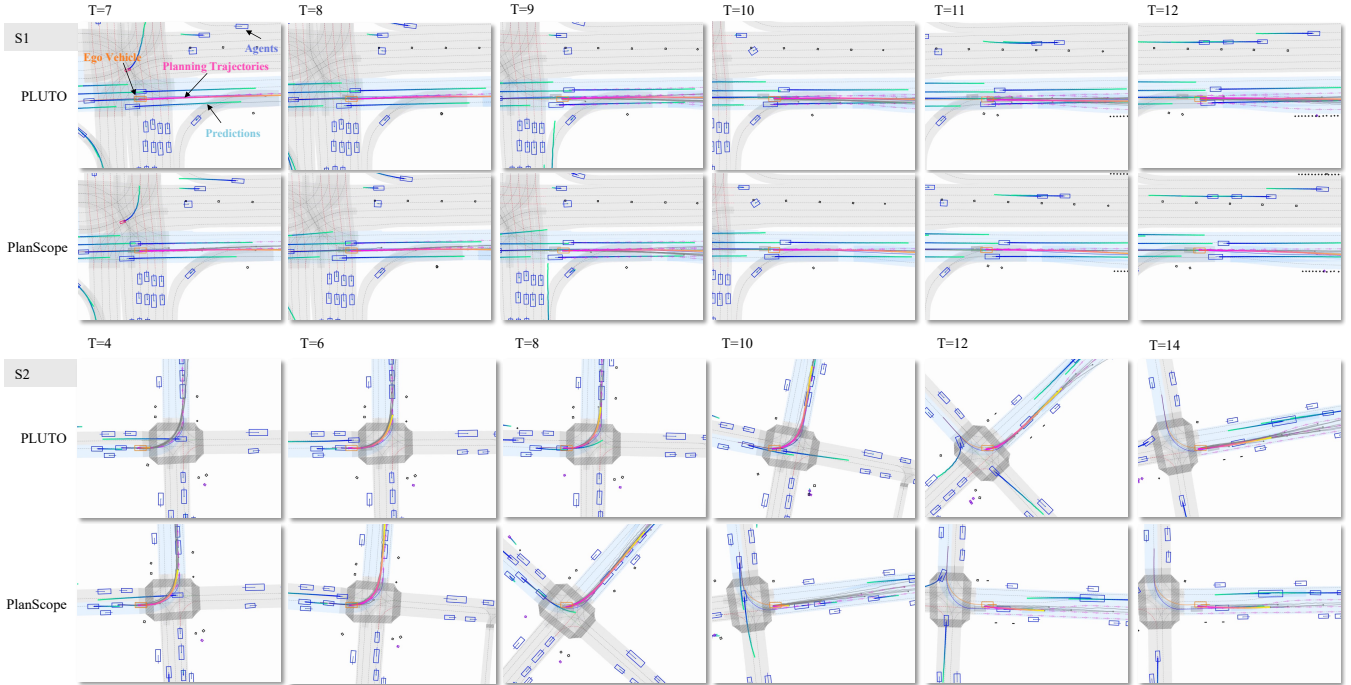


Fig. 5. In scenario **S1**, PLUTO plans to merge into the right lane, but it extensively focuses on future plans and does not pay attention to the vehicle approaching from the right rear, which causes the collision when $T=10$. PlanScope focused on the right rear and briefly made an evasive maneuver. In scenario **S2**, a typical left turn at an unprotected intersection, PLUTO fails to capture the sudden acceleration operation in the log replay, fearing the agent driving from opposite stopping in lane. This decision result in missing the action window and being rear-ended by the following vehicle, while PlanScope avoids the accident.

at level l are within the decision scope, supervising model training by

$$\mathcal{L}_{ds} = \frac{1}{N+2} \left(\sum_{l=0}^N (\|\mathcal{T}_D^l[:H_l] - \hat{\mathcal{T}}_D^l[:H_l]\|_2) + \|\mathcal{T}_A^N - \hat{\mathcal{T}}_A^N\|_2 \right),$$

where N is the count of detail level. The final query Q_{N+1} is then forwarded to the trajectory MLP decoder and scoring MLP decoder, yielding the multi-modal trajectory and the score by

$$\mathcal{T} = \text{MLP}(Q_{N+1}), \pi = \text{MLP}(Q_{N+1}),$$

$$\mathcal{L}_{reg} = \text{L1}_{\text{smooth}}(\mathcal{T}, \hat{\mathcal{T}}), \mathcal{L}_{cls} = \text{CrossEntropy}(\pi, \hat{\pi}),$$

where $\hat{\pi}$ is a one hot vector indicating the trajectory closest to logged trajectory. Finally, the overall training loss is designed as

$$\mathcal{L} = \mathcal{L}_{reg} + \mathcal{L}_{cls} + \mathcal{L}_{pre} + \mathcal{L}_{col} + \mathcal{L}_{ds}.$$

IV. EXPERIMENTS

A. Implementation Details

Our training is carried out in the nuPlan dataset [5], which comprises a training set of 25,000 scenarios. We evaluate our model’s performance against baseline models within the nuPlan challenge framework. In addition, we conduct an ablation study to determine the significance of each component within our model. The training is performed on a server equipped with four NVIDIA RTX 3090 GPUs. We employ the Adam optimizer, with a start learning rate of 0.0001, 3 warm-up epochs, and a batch size of 32, over the course of 25 training epochs. The PyTorch library is utilized for the model’s

implementation, with each training session approximately lasting 2 days.

Our evaluation is conducted on the **Val14** [25] subset of the nuPlan dataset, encompassing 1,090 validating scenarios. Each simulation entails a 15-second rollout at a frequency of 10 Hz. The evaluation score is derived using the official evaluation script provided by the nuPlan challenge. Our primary comparison metric is the Non-Reactive Closed-Loop Simulation (CLS-NR) driving score, which is more challenging as other vehicles do not avoid collisions with the ego vehicle. Besides, the future steps of our model is 80 while the history steps is 21. Both our model and **PLUTO** [21] are set to generate 6 modal trajectories. In our experiments, the maximum horizons of decision scope across levels are controlled by setting **DS Horizon**, which is denoted as h . Furthermore, we borrow the idea in [26] to facilitate the rapid implementation and execution of wavelet transformation in our experiments.

B. Comparison with Baselines

We conduct a comparative analysis of our method against several standard approaches, the comparative results are presented in Table I. **Log-Replay**, which entails a straightforward replay of expert trajectories, serves as a baseline reference. This demonstrates the capability of our simulator to accurately assess the performance of planning algorithms. **IDM** [27] employs the Intelligent Driver Model to maintain safe distances from other agents and adhere to the reference lane. **RasterModel**, introduced in [5], is a Convolutional Neural Network (CNN)-based planning model. **UrbanDriver** [28] is a vectorized planning model leveraging PointNet based

TABLE I
COMPARISON WITH BASELINE METHODS

Planner	Comfortness	Progress	Collisions	Speed Limit	Drivable	TTC	Score
Log-Replay	99.27%	98.99%	98.76%	96.47%	98.07%	94.40%	93.68%
IDM [27]	79.31%	86.16%	90.92%	97.33%	94.04%	83.49%	79.31%
RasterModel [5]	81.64%	80.60%	86.97%	98.03%	85.04%	81.46%	66.92%
UrbanDriver [28]	100.00%	80.83%	94.13%	91.58%	90.83%	80.28%	67.72%
PLUTO [21]	95.14%	87.13%	94.45%	97.87%	98.90%	90.92%	85.81%
PlanScope-h10 (ours)	96.24%	87.59%	94.59%	98.03%	98.99%	91.10%	85.94%
PlanScope-h20 (ours)	94.13%	85.39%	95.41%	98.48%	99.72%	93.94%	85.97%

TABLE II
ABLATION STUDY

Remark	IDD	DS Horizon	Score
No Additional Loss	-	-	81.47%
Decision Scope Absent	✓	0	84.69%
Position	✓	20	85.80%
Direct Velocity Loss	-	-	83.60%
Velocity	✓	20	86.77%
Velocity	✓	10	85.85%
Velocity	✓	30	85.76%
Velocity	✓	40	84.37%

polyline encoders and transformer architecture. **PLUTO** [21], our primary baseline, achieves state-of-the-art performance in the nuPlan planning challenge in April 2024. Naturally, we have excluded the rule-based trajectory selector, thereby demonstrating that our new model enhances the performance of the neural planner. Besides, we also eliminate the contrastive learning module, which is empowered by rule-based positive and negative sample construction. Our model, designated as **PlanScope**, is evaluated with maximum horizons of 10 and 20, decomposing velocity profile, and the maximum decomposition level N across experiments is 3. A qualitative comparison is depicted and introduced in Fig. 5. The results, as depicted in the table, indicate that the optimal total score of 85.97% is achieved at a horizon of 20. Notably, key safety metrics, including Time To Collision (**TTC**) and the absence of Ego-at-fault Collisions (**Collisions**), exhibit significant enhancements of 3.02% and 0.96%, respectively. At a horizon of 10, although the total score is marginally reduced, our model still surpasses the baseline across nearly all metrics, encompassing Progress Along Expert (**Progress**), Collisions, Speed Limit Compliance (**Speed Limit**), Drivable Area Compliance (**Drivable**), and **TTC**.

C. Ablation Study

To demonstrate the effectiveness of decision scope mechanism and IDD, ablation studies are conducted. The results are shown in Table II. In these studies, all models are trained on 20% of the dataset for 35 epochs and evaluated on the **Random14** [25] test set, comprising 249 scenarios. The ablation study encompasses the following configurations: In the first experiment, we train the baseline model without other additional peripheral loss achieving a CLS-NR score of 81.47%. For comparison, we implement the IDD to the model to demonstrate the effectiveness of iterative decoder, which results in a CLS-NR score of 84.69%, a 3.22% improvement

over the baseline. In the third experiment, we use the positional decision scope, enhancing the model’s CLS-NR score to 85.80%, a 4.33% increase from the baseline. In the fourth experiment, we introduce the direct velocity loss to the model, which yields a CLS-NR score of 83.60%, indicating a slight performance boost from emphasizing velocity differences. This result shows that emphasizing the velocity difference in demonstration can slightly improve the performance. In the experiment combining IDD with velocity decision scope, the model achieves a CLS-NR score of 86.77%, surpassing the baseline by 5.30% and the direct velocity loss by 3.17%. Further experiments vary the DS Horizon to explore the optimal effectiveness, and the results indicate that a DS Horizon of 20 achieves the best performance. Besides, with a total of 80 future time steps, a horizon of 40 represents level 0 detail data point count, effectively using all data for training. The DS mechanism exhibits peak performance at a horizon of 20, with a 2.40% decline in performance at a horizon of 40. This suggests that an overly extended planning scope can introduce excessive noise, and this confuses the model and degrades the planning performance, making the performance even worse than ignoring additional supervision.

V. CONCLUSIONS

This paper introduces a novel approach for planning future trajectories by extracting decisions across various frequency bands through wavelet decomposition, thereby enabling our model to discern the necessary decisions from log replays. We develop a mechanism by learning within the decision scope to accomplish this objective. References for multiple scope decisions are derived from the wavelet transformation of the expert trajectory data and utilized as an auxiliary loss for model training. The IDD technique recursively generates future trajectory details at multiple detail levels through the transformer. The experimental results indicate that our method outperforms baseline methods in achieving higher driving scores within the nuPlan dataset. Notably, in the small sample quantity comparison experiment, our method demonstrates a significant improvement of up to 5.77% in driving scores compared with the baseline. In the future, we plan to explore additional wavelet functions and potentially define a custom mother wavelet to more effectively capture driving information across different scales. Furthermore, we intend to integrate our method with perceptual information to optimize perception range, frequency, and resolution for key perceptual entities, thereby conserving computational resources and enhancing driving performance.

REFERENCES

- [1] S. Grigorescu, B. Trasnea, T. Cocias, and G. Macesanu, "A survey of deep learning techniques for autonomous driving," *Journal of Field Robotics*, vol. 37, no. 3, pp. 362–386, 2020.
- [2] C. Badue, R. Guidolini, R. V. Carneiro, P. Azevedo, V. B. Cardoso, A. Forechi, L. Jesus, R. Berriel, T. M. Paixao, F. Mutz, *et al.*, "Self-driving cars: A survey," *Expert Systems with Applications*, vol. 165, p. 113816, 2021.
- [3] T. Misu and Y.-T. Chen, "Toward reasoning of driving behavior," in *Proceedings of the IEEE International Conference on Intelligent Transportation Systems*, 2018, pp. 204–209.
- [4] A. Graps, "An introduction to wavelets," *IEEE Computational Science and Engineering*, vol. 2, no. 2, pp. 50–61, 1995.
- [5] H. Caesar, J. Kabzan, K. S. Tan, W. K. Fong, E. Wolff, A. Lang, L. Fletcher, O. Beijbom, and S. Omari, "nuPlan: a closed-loop ML-based planning benchmark for autonomous vehicles," in *Proceedings of the IEEE/CVF Conference on Computer Vision and Pattern Recognition ADP3 Workshop*, 2021.
- [6] M. Hoerger and H. Kurniawati, "An on-line POMDP solver for continuous observation spaces," in *Proceedings of the IEEE International Conference on Robotics and Automation*, 2021, pp. 7643–7649.
- [7] Y. Lee, P. Cai, and D. Hsu, "MAGIC: Learning Macro-Actions for Online POMDP Planning," in *Proceedings of the Robotics: Science and Systems*, 2021.
- [8] W. Ding, L. Zhang, J. Chen, and S. Shen, "Epsilon: An efficient planning system for automated vehicles in highly interactive environments," *IEEE Transactions on Robotics*, vol. 38, no. 2, pp. 1118–1138, 2021.
- [9] Y. Chen, J. Cheng, S. Wang, H. Liu, X. Mei, X. Yan, M. Tang, G. Sun, Y. Wen, J. Cai, *et al.*, "Enhancing campus mobility: Achievements and challenges of the snow lion autonomous shuttle," *IEEE Robotics & Automation Magazine*, 2024.
- [10] Y. Pan, Q. Lin, H. Shah, and J. M. Dolan, "Safe planning for self-driving via adaptive constrained ILQR," in *Proceedings of the IEEE/RSJ International Conference on Intelligent Robots and Systems*, 2020, pp. 2377–2383.
- [11] J. Mercat, T. Gilles, N. El Zoghby, G. Sandou, D. Beauvois, and G. P. Gil, "Multi-head attention for multi-modal joint vehicle motion forecasting," in *Proceedings of the IEEE International Conference on Robotics and Automation*, 2020, pp. 9638–9644.
- [12] M. Medhat, A. Abdel-hafiez, M. Hassan, M. Ali, and Z. Awaad, "A review on applications of the wavelet transform techniques in spectral analysis," in *Proceedings of the Conference on Nuclear and Particle Physics*, 2004.
- [13] A. H. Masquelin, N. Cheney, C. M. Kinsey, and J. H. Bates, "Wavelet decomposition facilitates training on small datasets for medical image classification by deep learning," *Histochemistry and Cell Biology*, vol. 155, no. 2, pp. 309–317, 2021.
- [14] Y. Zheng, S. He, R. Yi, F. Ding, B. Ran, P. Wang, and Y. Lin, "Categorizing car-following behaviors: wavelet-based time series clustering approach," *Journal of Transportation Engineering, Part A: Systems*, vol. 146, no. 8, p. 04020072, 2020.
- [15] B. I. Kwak, M. L. Han, and H. K. Kim, "Driver identification based on wavelet transform using driving patterns," *IEEE Transactions on Industrial Informatics*, vol. 17, no. 4, pp. 2400–2410, 2021.
- [16] R. V. Cowlagi and P. Tsotras, "Multiresolution motion planning for autonomous agents via wavelet-based cell decompositions," *IEEE Transactions on Systems, Man, and Cybernetics, Part B*, vol. 42, no. 5, pp. 1455–1469, 2012.
- [17] Z. Zhou, J. Wang, Y.-H. Li, and Y.-K. Huang, "Query-centric trajectory prediction," in *Proceedings of the IEEE/CVF Conference on Computer Vision and Pattern Recognition*, 2023, pp. 17 863–17 873.
- [18] J. Cheng, Y. Chen, X. Mei, B. Yang, B. Li, and M. Liu, "Rethinking imitation-based planners for autonomous driving," in *Proceedings of the IEEE International Conference on Robotics and Automation*, 2024, pp. 14 123–14 130.
- [19] C. R. Qi, H. Su, K. Mo, and L. J. Guibas, "PointNet: deep learning on point sets for 3d classification and segmentation," in *Proceedings of the IEEE Conference on Computer Vision and Pattern Recognition*, 2017, pp. 652–660.
- [20] J. Cheng, X. Mei, and M. Liu, "Forecast-MAE: self-supervised pre-training for motion forecasting with masked autoencoders," in *Proceedings of the IEEE/CVF International Conference on Computer Vision*, 2023, pp. 8679–8689.
- [21] J. Cheng, Y. Chen, and Q. Chen, "PLUTO: push the limit of imitation learning-based planning for autonomous driving," *arXiv preprint arXiv:2404.14327*, 2024.
- [22] N. Carion, F. Massa, G. Synnaeve, N. Usunier, A. Kirillov, and S. Zagoruyko, "End-to-end object detection with transformers," in *Proceedings of the European Conference on Computer Vision*, 2020, pp. 213–229.
- [23] R. Xin, J. Cheng, S. Wang, and M. Liu, "Velocity Field: an informative traveling cost representation for trajectory planning," in *Proceedings of the IEEE International Conference on Robotics and Biomimetics*, 2023, pp. 1–6.
- [24] J. Cheng, R. Xin, S. Wang, and M. Liu, "MPNP: Multi-Policy Neural Planner for Urban Driving," in *Proceedings of the IEEE/RSJ International Conference on Intelligent Robots and Systems*, 2022, pp. 10 549–10 554.
- [25] D. Dauner, M. Hallgarten, A. Geiger, and K. Chitta, "Parting with misconceptions about learning-based vehicle motion planning," in *Proceedings of the Conference on Robot Learning*, 2023.
- [26] M. Wolter, F. Blanke, J. Garcke, and C. T. Hoyt, "ptwt - The PyTorch Wavelet Toolbox," *Journal of Machine Learning Research*, vol. 25, no. 80, pp. 1–7, 2024.
- [27] S. Albeaik, A. Bayen, M. T. Chiri, X. Gong, A. Hayat, N. Kardous, A. Keimer, S. T. McQuade, B. Piccoli, and Y. You, "Limitations and improvements of the intelligent driver model," *SIAM Journal on Applied Dynamical Systems*, vol. 21, no. 3, pp. 1862–1892, 2022.
- [28] O. Scheel, L. Bergamini, M. Wolczyk, B. Osiński, and P. Ondruska, "Urban Driver: learning to drive from real-world demonstrations using policy gradients," in *Proceedings of the PMLR Conference on Robot Learning*, 2022, pp. 718–728.